CHEMISTRY OF MATERIALS

COMMUNICATION

pubs.acs.org/cm

# Growth of Metal Nanocrystals on Nanostructured Metal Oxides—Dramatic Effect of Antimony Doping

Engelbert Redel,[†] Eric Arsenault,[†] Paul G. O'Brien,[‡] Nazir P. Kherani,[‡] and Geoffrey A. Ozin*[,†]

[†]Lash Miller Chemical Laboratories, Department of Chemistry, University of Toronto, 80 St. George Street, Toronto, Ontario, Canada M5S 3H6

[‡]Department of Materials Science and Engineering, University of Toronto, 184 College Street Room 140, Toronto, Ontario, Canada M5S 3E4

Supporting Information

**KEYWORDS:** Antimony doped metal oxides, supported noble metal nanoparticles, enhanced nanoparticle loading

Metal oxides loaded with noble metal nanoparticles, like gold and platinum on titanium and tin dioxide have received much attention for decades. They have been found to have wide ranging applications in the chemical industry from heterogeneous catalysis to photocatalysis to chemical sensors and solar cells.[1] Interest in these composite materials originates from the combination of a catalytically active noble metal and a semiconductor metal oxide material.[2] Recently, metal oxide materials like nanocrystalline titania, *nc*$TiO_2$, self-assembled as inverse opals i-*nc*$TiO_2$-o have been used for slow-photon optical amplification of photochemical reactions,[3] where the reduction in the group velocity of light at the photonic band edge can be arranged to enhance the optical absorption of $TiO_2$ at the electronic absorption edge. This results in a photocatalytic enhancement that can be further increased by the synergistic catalytic effect of Pt nanoparticles deposited on the surface of i-*nc*$TiO_2$-o.[4] Additionally, $TiO_2$ can be successfully sensitized to visible light by doping with Sb providing a donor or acceptor level in the electronic bandgap of $TiO_2$.[5] Thus, the effect of Sb doping, as well as enabling a significantly higher level of metal loading, also allows one to extend the active wavelength range of photo catalytic reactions into the visible spectral region.[6] For certain heterogeneous catalytic reactions, it is desirable to prepare very high loadings up to 60 wt % metal nanoparticles,[7] e.g., for Reforming, FT (Fischer—Tropsch) synthesis or water-gas shift processes on hierarchically structured metal oxides like periodic mesoporous titania or macroporous titania or titania thin films[8] in which the metal nanoparticles have a uniform coverage, controllable size and a narrow nanoparticle size distribution. It was furher shown that deposition of higher loadings of noble metals on metal oxides can improve sensing properties[9] as well DSSC performance[10] of employed cathode materials by a higher density of catalytic sites. In the past, several approaches for the preparation of noble metal/metal oxide composites have been reported, including impregnation and deposition-precipitation, photodeposition, electrodeposition, sputtering and colloidal chemistry techniques.[11,12] Although these approaches are relatively straightforward, it is often challenging to control metal particle size, distribution, and loading.[13]

Herein, we present a general method to dramatically increase the loading of noble metal nanoparticles in inverted metal oxide opals through Sb doping of the metal oxide. In this study the method is exemplified by the growth of some noble metal nanoparticles on Sb doped i-*nc*Sb:$TiO_2$-o and i-*nc*Sb:$SnO_2$-o films. As precursors we employed $SnCl_4$ and $Ti(O^tBu)_4$ with $Sb(OAc)_3$ as the Sb doping source.[14] Growth of noble metal nanoparticles was performed using the deposition-precipitation technique in the pH range 8.9—9.1 and simple metal salt precursors ($10^{-4}$ mol) at 80 °C for 2 h.[13] Detailed information for the synthesis and characterization of Sb doped i-*nc*Sb:$TiO_2$-o and i-*nc*Sb:$SnO_2$-o supported noble metal nanoparticles is included in the Supporting Information, see Figures S3 and S4.

The method reported herein has certain advantages: (i) the noble metal nanoparticles are uniformly distributed over the metal oxide support with an average size that ranges from 3.7 - 6.7 nm and a narrow size distribution, see Table 1; (ii) an additional reducing agent is not required to generate the metal nanoparticles, avoiding the introduction of adventitious impurities; (iii) the method works well under mild conditions and can be extended to a range of transition metal nanoparticles on the two kinds of Sb doped metal oxides mentioned above. STEM measurements showed that in all as-synthesized samples of Sb doped i-*nc*Sb:$TiO_2$-o and i-*nc*Sb:$SnO_2$-o (with, Sb doping around ~2 wt %) all surfaces appeared to be uniformly and densely covered with noble metal nanoparticles (M NPs) in contrast to the less uniform sparse coatings observed for the nondoped samples Figure 1a—c (also see the Supporting Information, Figures S6—S16). It should be mentioned that M NP formation occurs only after calcination at 350 °C under $N_2$ for 4 h. STEM measurements show no M NPs from the noncalcined samples after the deposition process. In the case of Au or Ag NPs the characteristic Surface Plasmon Resonance SPR bands were detected only after the calcination treatment, see the Supporting Information, Figures S6 and S17—19.

**Received:** November 16, 2010
**Revised:** February 1, 2011
**Published:** February 16, 2011

**Table 1. Different Noble Metal Nanoparticles M NPs Supported on Sb-Doped i-*nc*Sb:$TiO_2$-o and i-*nc*Sb:$SnO_2$-o**

| | nobel metal nanoparticles | metaloxide support | STEM median diameter (nm) ($\sigma$ range (nm)) |
|---|---|---|---|
| 1 | Au-NPs | i-*nc*Sb:$SnO_2$-o | 5.80 ± 1.31 (4.3−7.4) |
| 2 | Ag-NPs | i-*nc*Sb:$SnO_2$-o | 5.50 ± 1.67 (2.8−6.9) |
| 3 | Pt-NPs | i-*nc*Sb:$SnO_2$-o | 3.82 ± 0.84 (2.0−5.3) |
| 4 | Au-NPs | i-*nc*Sb:$TiO_2$-o | 6.21 ± 1.47 (4.1−8.7) |
| 5 | Ag-NPs | i-*nc*Sb:$TiO_2$-o | 4.38 ± 1.26 (2.6−6.2) |
| 6 | Pt-NPs | i-*nc*Sb:$TiO_2$-o | 3.68 ± 0.70 (2.3−4.8) |
| 7 | Ag/Au-NPs | i-*nc*Sb:$TiO_2$-o | 6.71 ± 1.20 (4.2−8.2) |

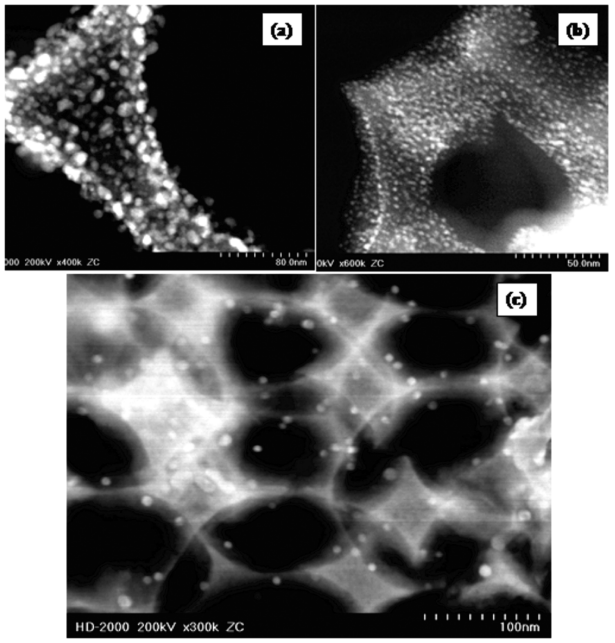


**Figure 1.** (a) Au NPs on a fragment of i-*nc*Sb:$SnO_2$-o, (b) Au NPs on Sb doped i-*nc*Sb:$TiO_2$-o, (c) Au-NPs on undoped i-*nc*$TiO_2$-o.

It is believed that the formation of noble metal NPs most likely begins with the anchoring of the as-deposited light yellow-orange ionic gold species $[Au(OH)_x]$[15] to the abundance of free OH groups on the oxide surface, see the Supporting Information, Figures S20 and S21. Powder X-ray diffraction, PXRD, measurements and Rietveld refinement phase analysis confirmed the existence of the nanocrystalline Anatase in i-*nc*$TiO_2$-o, in combination with nanocrystalline Au at a loading level of 40.5 wt %, see the Supporting Information, Figure S1. Mean sizes for Au NPs are 8.8 ± 1.2 nm. Confirmation of these high Au NP loadings comes from quantitative gold analysis on five samples using AAS which defines a loading of 40−49 wt % and represents a roughly 3-fold increase of the Au loading for the Sb-doped i-*nc*Sb:$TiO_2$-o compared to the undoped i-*nc*$TiO_2$-o samples, see the Supporting Information, Table S2.

XPS measurements define a monotonic increase of the Sb dopant concentration in the samples based on the increase of the $Sb3d_{3/2}$ peak, as well the formation of a new $Au(OH)_x$ species seen from the O1s and Au4f peaks during the desposition process and the formation of Au(0) NPs during the calcination process

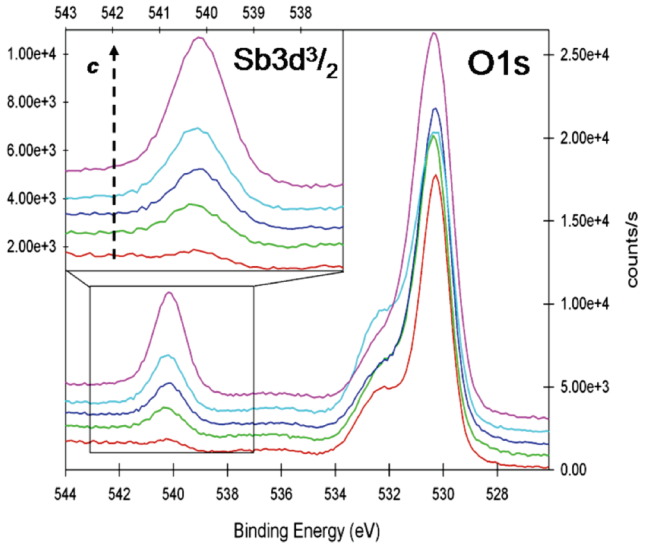


**Figure 2.** XPS results: Sb doping dependence (0.2−5 mg; c[Sb] ≈ 0.2−5 wt %) in the O1s and $Sb3d_{3/2}$ region of i-*nc*$TiO_2$-o. The broad peak at 531−534 eV represents the TiOH groups on the $TiO_2$ surface, whereas the higher-energy O peak at 528−532 eV indicates the lattice oxygen.

see Figure 2 and the Supporting Information, Figures S20 and 21. In this context, I−V measurements, discussed below show an increase in the electrical conductivity of i-*nc*Sb:$TiO_2$-o films due to an increase in the Sb dopant concentration.

An explanation of the aforementioned Sb doping effect is based on a model[16] of a uniform substitution of $Sb^{5+}$ (60.0 pm)[5] for $Ti^{4+}$ (60.5 pm)[16] into the $TiO_2$ lattice; also see the Supporting Information, Figure S5 and S6. The $Sb^{5+}$ species are formed in the calcination step through oxidation of the incorporated $Sb^{3+}$ (76.0 pm)[16] to $Sb^{5+}$. The $Sb3d_{3/2}$ XPS peak at 540.5 eV is symmetrical, Figure 2, and devoid of fine structure, from which we deduce the existence of a dominant $Sb^{5+}$ species[17] from different thermal treatments. This finding provides the basis of formulating a model for the observed uniform M NP coating on Sb doped i-*nc*Sb:$TiO_2$-o. For detailed information, see the Supporting Information, Figures S2−S16.

The proposal is that $Sb^{5+}$ ions can be isomorphously substituted into the $TiO_2$ lattice to create [Ti−OH−Sb, HO−Ti−O−Sb, Ti−O−Sb−OH] sites bearing terminal and bridging OH groups, which under basic synthesis conditions (pH ∼9) can be deprotonated to generate a local negative charge. Anchoring of the $M(OH)_x$ precursor can occur by coordination to surface $Sb^{5+}$ sites (higher Lewis acidity than $Ti^{4+}$) or with Sb−OH species (higher Brønsted acidity than Ti−OH species on metal oxide surfaces, $pK_a$ [Sb(V)Oxides] ≈ 0.4 ≪ $pK_a$ [Ti(IV)Oxides] 4−8).[18] This could explain the effect of Sb doping on the enhanced loading of noble NPs by favoring the binding of the $M(OH)_x$ precursor on the Sb-doped relative to the undoped i-*nc*$TiO_2$-o surface. Another explanation is based on making the i-*nc*$TiO_2$-o surface "more electron rich" by introducing Sb dopants that are expected to function as *n*-dopants (see Figure 3) and therefore helping to more efficiently anchor $M(OH)_x$ precursor and/or the reduction/calcination process. Also as the precursor is reduced to M(0) in the calcination step, the stronger Lewis acidity of the incorporated $Sb^{5+}$ surface species results in a stronger interaction with M(0) and therefore impedes its diffusion and agglomeration to M NPs, thereby


dx.doi.org/10.1021/cm1032964 |*Chem. Mater.* 2011, 23, 1353–1355

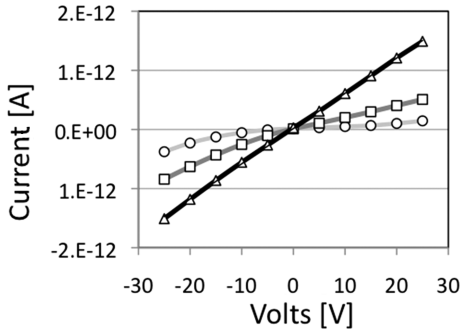


**Figure 3.** $I-V$ curves for i-*nc*$TiO_2$-o film that are undoped (circles), or doped with either 5 mg (squares) or 10 mg (triangles) of the dopant precursor. Measurements are taken from −25 V to +25 V in increments of 5 V.

keeping them small and well-dispersed on the metal oxide surface, see Table 1, Figure 1a,b and the Supporting Information, Figures S6−S16 and S19.

We have performed current−voltage measurements on our Sb-doped i-*nc*$TiO_2$-o films, Figure 2, and Au NP-loaded Sb-doped i-*nc*$TiO_2$-o as seen in Figure 1b and Table 1. Specifically, i-*nc*Sb:$TiO_2$-o doped with varying levels of Sb were prepared on highly resistive glass slides (corning 1737). Two rectangular coplanar aluminum contacts (0.25 cm × 0.5 cm), spaced apart by 400 $\mu$m were then deposited onto each sample via physical vapor deposition. The current through these films was then measured, using a Keithley 6517 electrometer, as different voltage biases were applied across the pair of aluminum contacts, for further details see the Supporting Information.

The $I-V$ measurements, shown in Figure 3, imply that $Sb^{5+}$ dopant atoms are incorporated into the $TiO_2$ lattice. The conductivity of the i-*nc*Sb:$TiO_2$-o films prepared with 5 mg of dopant precursor is greater than that of undoped films and the i-*nc*Sb:$TiO_2$-o films with 10 mg of dopant precursor exhibit the largest conductivity. The Sb dopants are expected to function as *n*-dopants thereby increasing the electron carrier concentration in the host $TiO_2$ matrix, increasing the conductivity of the i-*nc*Sb:$TiO_2$-o films. Furthermore, as the i-*nc*Sb:$TiO_2$-o films are doped to a greater extent, their $I-V$ curves become more Ohmic.

In conclusion, we have found and explained that Sb *n*-doping dramatically increases noble metal NP loading on titanium and tin dioxide structured as inverted opals. The method seems to apply equally well to other transition metal nanoparticles, like Rh, Ir, Ru, Pd, Pt on these Sb-doped metal oxide surfaces. High metal nanoparticle loading nanostrutured metal oxides of the kind described in this report provide interesting opportunities for heterogeneous catalysis, photocatalysis, chemical sensors, and solar cell applications.

## ■ ASSOCIATED CONTENT

**Ⓢ Supporting Information.** Synthesis and characterization information for noble metal nanoparticles (PXRD, STEM, XPS and UV−VIS−NIR) grown on inverted metal oxide opals as well as measurement/analysis data (PDF). This material is available free of charge via the Internet at http://pubs.acs.org/.

## ■ AUTHOR INFORMATION

**Corresponding Author**
*E-mail: gozin@chem.utoronto.ca.

## ■ ACKNOWLEDGMENT

G.A.O. is Government of Canada Research Chair in Materials Chemistry and Nanochemistry. He is deeply indebted to NSERC for strong and sustained support of his research. E.R. thanks the Alexander von Humboldt (AvH) Foundation for a Feodor Lynen Postdoctoral fellowship. E.A. and P.G.O. thank NSERC for a graduate fellowship (CGS). The authors thank Dr. Srebri Petrov for PXRD measurements, Dr. Peter Broderson for XPS measurements and analysis, and Dan Mathers for advising on AAS measurements.

## ■ REFERENCES

(1) (a) Choi, S. Y.; Lee, B.; Carew, D. A.; Mamak, M.; Peiris, F. C.; Speakman, S.; Chopra, N.; Ozin, G. A. *Avd. Funct. Mater.* **2006**, *16*, 1731. (b) Garcia, M. F.; Anderson, J. A. *Supported Metals in Catalysis*; Catalytic Science Series; Imperial College Press: London, 2005; Vol. 5, pp 1−380.

(2) (a) Chen, M. S.; Goodman, D. W. *Acc. Chem. Res.* **2006**, *39*, 739. (b) Corma, A.; Serna, P.; Garca, H. *J. Am. Chem. Soc.* **2007**, *129*, 6358. (c) Xie, Y.; Ding, K.; Lui, Z.; Tao, R.; Sun, Z.; Zhang, H.; An, G. *J. Am. Chem. Soc.* **2007**, *131*, 6648.

(3) (a) Chen, J. I. L.; von Freymann, G.; Choi, S. Y.; Kitaev, V.; Ozin, G. A. *Adv. Mater.* **2006**, *18*, 1915. (b) Chen, J. I. L.; von Freymann, G.; Choi, S. Y.; Kitaev, V.; Ozin, G. A. *J. Mater. Chem.* **2008**, *18*, 369. (c) Chen, J. I. L.; von Freymann, G.; Kitaev, V.; Ozin, G. A. *J. Am. Chem. Soc.* **2007**, *129*, 1196.

(4) Chen, J. I. L.; Loso, E.; Ebrahim, N.; Ozin, G. A. *J. Am. Chem. Soc.* **2008**, *130*, 5420.

(5) Takagi, H.; Fujishiro, Y.; Awano, M. *J. Mater. Sci.* **2001**, *36*, 949.

(6) (a) Choi., W. Y.; Termin, A.; Hoffman, M. R. *J. Phys. Chem.* **1994**, *98*, 13669. (b) Di, P. A.; Marcí, G.; Palmisano, L.; Schiavello, M.; Uosaki, K.; Ikeda, S.; Ohtani, B. *J. Phys. Chem. B* **2002**, *106*, 637.

(7) Wang, S.; Lu, G. Q. *Energy Fuels* **1996**, *10*, 896.

(8) Ramanathan, S. *Thin Film Metal Oxides*; Springer-Verlag: Weinheim, Germany, 2010; pp 281−301.

(9) Shimizu, J.; Matsunaga, N.; Hyodo, T.; Egashira, M. *Sens. Actuators, B* **2001**, *77*, 35.

(10) Calandra, P.; Calogero, G.; Sinopoli, A.; Gucciardi, P. G. *Int. J. Photoenergy* **2010**, 109495.

(11) (a) Yan, W. F.; Shannon, M. M.; Pan, Z. W.; Steven, H. O.; Dai, S. *J. Am. Chem. Soc.* **2005**, *127*, 10480. (b) Li, J.; Zeng, H. C. *Chem. Mater.* **2006**, *18*, 4270.

(12) (a) Bond, G. C.; Louis, C.; Thompson, D. T. *Catalysis by Gold*; Catalytic Science Series; Imperial College Press,: London, 2006; Vol. 6, pp 72−120. (b) Heiz, U.; Landman, U., *Nanocatalysis*; Springer-Verlag: Weinheim, Germany, 2006, pp 377−394.

(13) (a) Wolf, A.; Schüth, F. *Appl. Catal., A* **2002**, *226*, 1–13. (b) Moreau, F.; Bond, G. C.; Taylor, A. O. *J. Catal.* **2005**, *231*, 105.

(14) (a) Hou, K.; Puzzo, D.; Helander, M. G.; Lo, S. S.; Bonifacio, L. D.; Wang, W.; Lu, Z.-H.; Scholes, G. D.; Ozin, G. A. *Adv. Mater.* **2009** *21*, 2492. (b) Wang, Y. D.; Djerdj, I.; Antonietti, M.; Smarsly, B. *Small* **2008**, *4*, 1656. (c) Wang, Y. D.; Djerdj, I.; Smarsly, B.; Antonietti, M. *Chem. Mater.* **2009**, *21*, 3202.

(15) Kydd, R.; Scott, J.; Teoh, W. Y.; Chiang, K.; Amal, R. *Langmuir* **2010**, *26*, 2099.

(16) (a) Chen, X.; Mao, S. S. *Chem. Rev.* **2007**, *107*, 2891. (b) Bechstein, R.; Kitta, M.; Schütte, J.; Kühnle, A.; Onishi, H. *J. Phys. Chem. C* **2009**, *113*, 13199.(c) Bechstein, R.; Kitta, M.; Schütte, J.; Onishi, H.; Kühnle, A. *Nanotechnology* **2009**, *20*, 264003 (7pp).

(17) http://srdata.nist.gov/xps/ (accessed September 28, 2008).

(18) (a) Brunelle, J. P. *Pure Appl. Chem.* **1978**, *50*, 1211.(b) Rosenholm, J. B.; Lindén, M. In *Handbook Surface and Colloid Chemistry*; Taylor & Francis Group: Oxford, U.K., 2009; pp 440−494.